ARTICLE

Molecular motion of halogenated ethylammonium / [18]crown-6 supramolecular ions in nickel dithiolate magnetic crystals

Received 00th January 20xx,
Accepted 00th January 20xx

DOI: 10.1039/x0xx00000x

Naohiro Hasuo,[a] Kiyonori Takahashi,*[a,b] Ichiro Hisaki,[c] Kenta Kokado,[a,b,d] Takayoshi Nakamura*[a,b]

Supramolecular cations, consisting of ethylammonium derivatives (X-CH_2CH_2-NH_3^+) complexed with [18]crown-6, were incorporated into $[Ni(dmit)_2]^-$ crystals in order to promote molecular motion. Crystals of (X-CH_2CH_2-NH_3^+)([18]crown-6)$[Ni(dmit)_2]^-$ (**1**: X=H, **2**: X=F, **3**: X=Cl and **4**: X=Br) were prepared for this purpose. Although large amplitude molecular motions do not occur in crystal **1**, dynamic disorder of F-CH_2 groups takes place between two sites in crystal **2**. Similar disorder of Cl-CH_2 groups along with rotation of [18]crown-6 molecules also exists in crystal **3**. Crystal **4** exhibits dynamic disorder of Br-CH_2-CH_2 groups between four sites. This is especially the case for crystal **4** which undergoes a distinct dielectric response with relaxer-like behavior in the temperature dependence of the dielectric loss tangent. Interactions between $[Ni(dmit)_2]^-$ ions in all crystals are antiferromagnetic, and the magnitudes of the interactions are qualitatively consistent with the strength of intermolecular interactions estimated from transfer integrals, where interactions within $[Ni(dmit)_2]^-$ dimers are the larger than the others in all crystals.

Introduction

Although rare, order-disorder type molecular motion of alkyl chains has been observed to take place in closely packed crystals, and to play an important role in governing unique functions such as ferroelectricity.[1-13] For example, ethyl groups in $C_2H_5NH_3^+$ moieties in $(C_2H_5NH_3^+)_2[BiBr_5]$ crystals at room temperature[11] display orientational disorder between two sites. In the frozen state at 160 K, the crystals undergo a phase transition associated with a change of the crystal space group from non-polar *Aeam* to polar *Pca*2_1. Moreover, in the low-temperature phase, the ethyl groups in $(C_2H_5NH_3^+)_2[BiBr_5]$ are uniformly oriented, and can be altered by applying an external electric field in association with a ferroelectric hysteresis with a polarization of 0.01 μC cm^{-1} at 156 K. Thus, ferroelectricity is generated by controlling the orientation of the ethyl groups.[11]
Introduction of dipole moments in mobile groups is an effective approach to create materials that display efficient ferroelectric, piezoelectric and pyroelectric responses. One strategy to accomplish this goal involves the introduction polar groups into alkyl chains.[7,14–18] For example, the (TMA^+)($FeBr_4^-$) (TMA = tetramethylammonium$^+$) crystal belongs to the highly symmetric space group of *Pbcm*. Introduction of a halogen into one of the methyl groups creates $[(Me)_3N^+(CH_2\text{-}X)](FeBr_4^-)$ (X = F, Cl, Br, and I) crystals that are polar and display spontaneous polarization at room temperature.[18] The dipole moments in these crystals do not cancel each other, which results in multiaxial ferroelectric ordering. The (TMA^+)($FeBr_4^-$) and $[(Me)_3N^+(CH_2\text{-}X)](FeBr_4^-)$ crystals at higher temperatures display plastic crystalline phases. Both the cations and the anions in the crystals possess pseudo spherical structures, which enables them to rotate freely. In the case of $[(Me)_3N^+(CH_2\text{-}X)](FeBr_4^-)$, this leads to multi-directional polarization. However, while effective, it is generally quite difficult to create systems in which molecular motion takes place in closely-packed crystals.
In past efforts, we utilized supramolecular cation structures to introduce spaces in crystals that enable molecular motion to occur.[19–23] One strategy of creating space in crystals is to utilize a cage structure composed of covalent and/or coordination bonds. However, this protocol usually requires multistep synthetic schemes.[24–33] In contrast, supramolecular structures formed by self-assembly in crystals are sufficiently flexible to create the space required for molecular motion.[34–42] For example, in the crystal of (*m*-$FAni^+$)(dibenzo[18]crown-6)$[Ni(dmit)_2]^-$ (*m*-$FAni^+$ = *m*-fluoroanilinium$^+$, $dmit^{2-}$ = 1,3-

[a] *Graduate School of Environmental Science, Hokkaido University, N10W5, Kita-ku, Sapporo 060-0810, Japan*
[b] *Research Institute for Electronic Science (RIES), Hokkaido University, N20W10, Kita-ku, Sapporo, 001-0020, Japan*
[c] *Graduate School of Engineering Science, Osaka University, 1-3, Machikaneyama, Toyonaka, Osaka, 560-8531, Japan*
[d] *JST-PRESTO, Honcho 4–1-8, Kawaguchi, Saitama 332-0012, Japan.*
E-mail: (KT) ktakahashi@es.hokudai.ac.jp, (TN) tnaka@es.hokudai.ac.jp
Electronic Supplementary Information (ESI) available: See DOI: 10.1039/x0xx00000x

dithio-2-thione-4,5-dithiolate^{2-}), the *m*-FAni^{+} and dibenzo[18]crown-6 moieties form a supramolecular rotor structure through hydrogen bonding interactions.[42] In the rotor, *m*-FAni^{+} displays flip-flop type rotational motion around the CN bond, enabling inversion of the dipole moment to take place by applying an external electric field with a ferroelectric transition occurring at 346 K. This example demonstrates the great potential of employing the supramolecular approach using crown ethers to enable molecular motion within tightly packed crystals.[43]

In the study described below, we applied the supramolecular approach to design crystals of (X-CH_2CH_2-NH_3^+)([18]crown-6)[Ni(dmit)$_2$]$^-$ (**1**: X = H, **2**: X = F, **3**: X = Cl, and **4**: X = Br), which contain alkylammonium halide chains (X-CH_2CH_2-NH_3^+). As in the case of (*m*-FAni$^+$)(dibenzo[18]crown-6)[Ni(dmit)$_2$]$^-$, crystals **1-4** contain [Ni(dmit)$_2$]$^-$ with S = 1/2 spin as the counter anion. An investigation of the physical properties clearly showed the effectiveness of the supramolecular approach in that the halogenated alkyl chains in **2-4** display motional freedom within the crystals. Especially noteworthy was the observation that Br-CH_2CH_2-NH_3^+ exhibits dynamic disorder between four sites. In addition, the results showed that morphology and size of supramolecular cations have significant effects on the arrangement and magnetic behavior of [Ni(dmit)$_2$]$^-$.

Experimental

General

All reagents were used without further purification. Elemental analyses were carried out by using a CHN analyzer (CE440, Exeter Analytical, Inc.) at the Instrumental Analysis Division, Equipped Management Center, Creative Research Institution, Hokkaido University.

Crystal Preparation

Precursor of (TBA$^+$)[Ni(dmit)$_2$]$^-$ (TBA$^+$ = tetra-*n*-butylammonium$^+$) was prepared using a literature procedure.[44] Single crystals of (H-CH_2CH_2-NH_3^+)([18]crown-6)[Ni(dmit)$_2$]$^-$ (**1**), (F-CH_2CH_2-NH_3^+)([18]crown-6)[Ni(dmit)$_2$]$^-$ (**2**), (Cl-CH_2CH_2-NH_3^+)([18]crown-6)[Ni(dmit)$_2$]$^-$ (**3**) and (Br-CH_2CH_2-NH_3^+)([18]crown-6)[Ni(dmit)$_2$]$^-$ (**4**) were prepared by slow evaporation from a mixture of acetonitrile and methanol at room temperature. Specifically, a green solution of (TBA)[Ni(dmit)$_2$] (0.050 mol) in acetonitrile (40 mL) was slowly added to a colorless solution of each X-CH_2CH_2-$NH_3^+Cl^-$ salt (0.10 mol) in methanol (5 mL). After several days, block-shaped black single crystals were produced (yields: 43.5 mg, 78.0% for crystal **1**, 30.0 mg, 52.6% for crystal **2**, 27.3 mg, 48.5% for crystal **3**, and 23.2 mg, 37.3% for crystal **4**). Anal. Calcd (%) for $C_{20}H_{32}NO_6NiS_{10}$ (M.W. 761.77): C, 31.53; H, 4.23 N, 1.84. Found: C, 31.37; H, 4.08; N, 1.76 (crystal **1**), for $C_{20}H_{31}NO_6FNiS_{10}$ (M.W. 779.77): C, 30.80; H, 4.01 N, 1.80. Found: C, 30.78; H, 3.89; N, 1.73 (crystal **2**), for $C_{20}H_{31}NO_6ClNiS_{10}$ (M.W. 796.22): C, 30.17; H, 4.01 N, 1.80. Found: C, 30.00; H, 3.83; N, 1.81 (crystal **3**), and for $C_{20}H_{31}NO_6BrNiS_{10}$ (M.W. 840.73): C, 28.55; H, 3.62 N, 1.61. Found: C, 28.57; H, 3.72; N, 1.67 (crystal **4**).

Crystal Structure Determination

Temperature-dependent X-ray crystallographic analysis of single crystals **1**, **2**, **3** and **4** was performed using a Rigaku XtaLab Synergy diffractometer with a single microfocus Mo Kα X-ray radiation source (PhotonJet-S), equipped with a Hybrid Pixel (HyPix) Array detector (HyPix-6000HE). Multi-scan absorption corrections were applied to the reflection data. A single crystal was mounted on Mounted CryoLoop (Hampton Research) with Paratone® 8277 (Hampton Research). Data collection, cell refinement, and data reduction were carried out with CrysalisPRO (Rigaku Oxford Diffraction, 2017). In each case, the initial structure was solved by using SHELXT,[45] and structural refinement was performed by using full-matrix least-squares techniques on F2 using OLEX2 package.[46] Anisotropic refinement was applied to all atoms except for hydrogens. CCDC deposition numbers are summarized in Tables S1 ~ S5.

Dielectric Measurement

Temperature- and frequency-dependent dielectric constants (ε_1) and dielectric loss tangents (tan δ) were measured using an impedance analyzer 4294A (Agilent) with the four-probe AC impedance method at a frequency range from $10^{3.5}$ to 10^6 Hz with $10^{0.5}$ Hz increments. Each crystalline sample was powdered with agate milk stick and pelletized with a shaper. Gold paste (No. 8556, Tokuriki Chemical Research Co., Ltd.) and 10 μm ϕ gold wires (Nilaco Corp.) were used for electrical contacts between sample and electrical wire from the device. Temperature was controlled using a cryostat with a temperature controller model 331 (Lake Shore Cryotronics Inc.).

Magnetic Measurements

The temperature dependence of the magnetic susceptibility (χ_m) was measured in the range of 2 to 300 K under a constant magnetic field of 1 T using a MPMS 3 SQUID magnetometer (Quantum Design). Before the measurement, the diamagnetic susceptibility of the sample holder (plastic wrap) was measured under the same conditions, and the diamagnetic component of the sample holder was subtracted from value obtained including the sample. Moreover, the diamagnetic component (–0.000399, –0.000429, –0.000416, and –0.000427 cm^3 mol^{-1} for crystals **1**, **2**, **3**, and **4**, respectively) were subtracted from the obtained data. Paramagnetic impurities which obey the Curie–Weiss law (0.00182, 0.00324, 0.0110, and 0.00211 of Curie constant for crystals **1**, **2**, **3**, and **4**, and Weiss temperature of 0 K) were subtracted from obtained data for Figure 6.

Calculation of Transfer Integrals

The extended Hückel molecular orbital method along with the tight binding approximation was applied to calculate the transfer integral (*t*) between $[Ni(dmit)_2]^-$ anions. The lowest unoccupied molecular orbital of $[Ni(dmit)_2]^-$ molecule was used as the basic function.[47] According to the literature, semi-empirical parameters of Slater-type atomic orbitals were obtained.[47] It was assumed that the *t* values between each pair of molecules are proportional to the overlap integrals (*S*) according to the equation $t = -10\ S$ eV.

Results and discussion

Crystal structure

The results of crystallographic analysis show that crystals **1**-**4** have the same crystal system (triclinic) and space group (*P*-1). The crystal structure of **1** at 113 K is displayed in Figure 1. Each molecule of X-CH_2CH_2-NH_3^+, [18]crown-6, and $[Ni(dmit)_2]^-$ is crystallographically independent in the crystal. In each crystal, $[Ni(dmit)_2]^-$ exists as dimers that are arranged one-dimensionally along the *c*-axis. The $[Ni(dmit)_2]^-$ one-dimensional arrays are aligned in the *ac* plane to form two-dimensional layers. The X-CH_2CH_2-NH_3^+ and [18]crown-6 components create a 1:1 supermolecule through hydrogen bonding interactions between the NH_3 group of X-CH_2CH_2-NH_3^+ and oxygen atoms of [18]crown-6. Each supramolecular cation has contacts that are shorter than the sum of van der Walls radii with the adjacent supramolecular cation, leading to generation of cation pairs. The supramolecular cation pairs in crystal **1** are arranged one-dimensionally along the *c* axis and aligned between the $[Ni(dmit)_2]^-$ layers.

Although the overall crystal structures of crystals **1**-**4** are similar (Figure S5 in electronic supplementary information (ESI)), interactions between the supermolecules within the supramolecular pairs are significantly different especially in crystal **3**. In crystals **1**, **2** and **4**, adjacent [18]crown-6 molecules in each pair are arranged in a gear-like manner through C-H•••O interactions (Figure 2 and for detail see Table S6 in SI). On the other hand, in crystal **3**, [18]crown-6 is disordered between two sites with an occupancy ratio of 0.405(2): 0.505(2). The occupancy ratio is temperature dependent

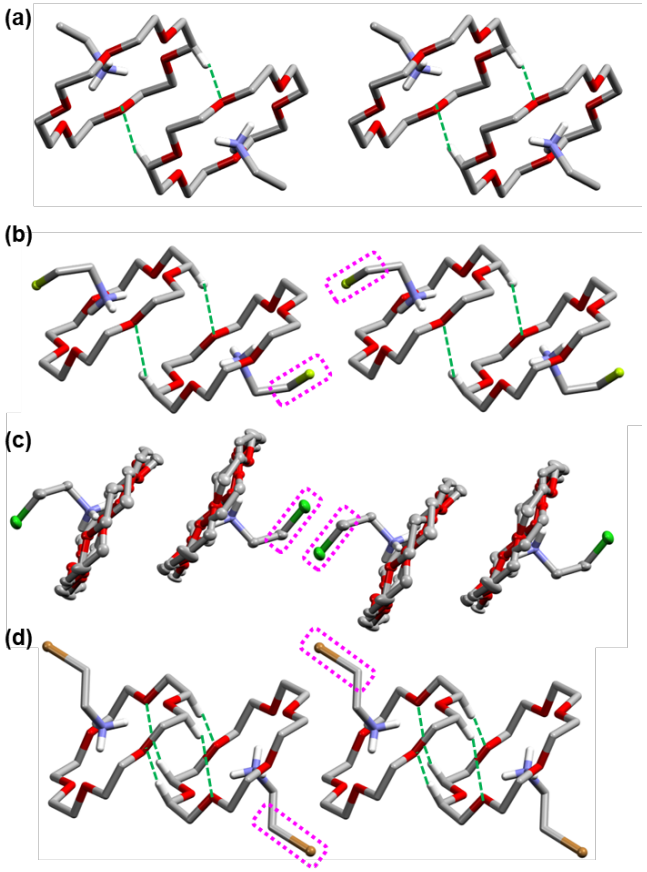

Figure 2 One-dimensional array of supramolecular cations in crystals (a) **1** at 106 K, (b) **2** at 93 K, (c) **3** at 113 K, and (d) **4** at 106 K. Hydrogen atoms are omitted for clarity except hydrogen atoms involved in N-H•••O hydrogen bonds, and C-H•••O interactions (green dotted lines). White, light-blue, red, yellow, green and brown colored atoms correspond to carbon, hydrogen, nitrogen, oxygen, fluorine, chlorine, and bromine, respectively. X-CH_2 groups between the pair of supramolecule in crystals **2**-**4** are encircled by pink dotted square. Two of three disordered sites of Br-CH_2-CH_2 are also omitted in **4**.

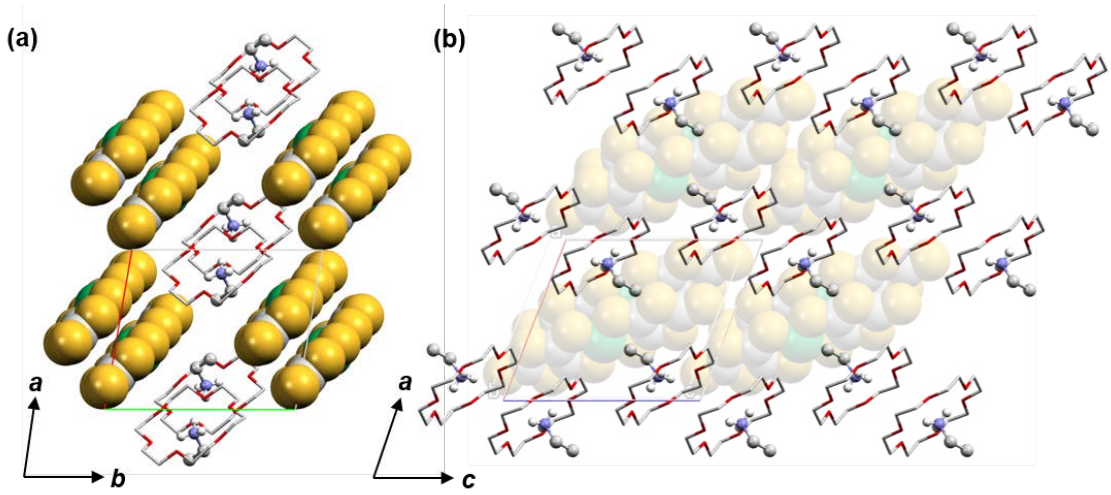

Figure 1 Packing structure of **1** viewed along the (a) *c* and (b) *b* axis at 113 K. Sulfur, carbon, and nickel atoms in $[Ni(dmit)_2]^-$ are indicated by yellow, grey, and green, respectively, in the space-filling model. H-CH_2CH_2-NH_3^+ and [18]crown-6 are indicated by ball and stick, and wire models, respectively. Hydrogen atoms are omitted for clarity except hydrogen atoms bonded to nitrogen atom.

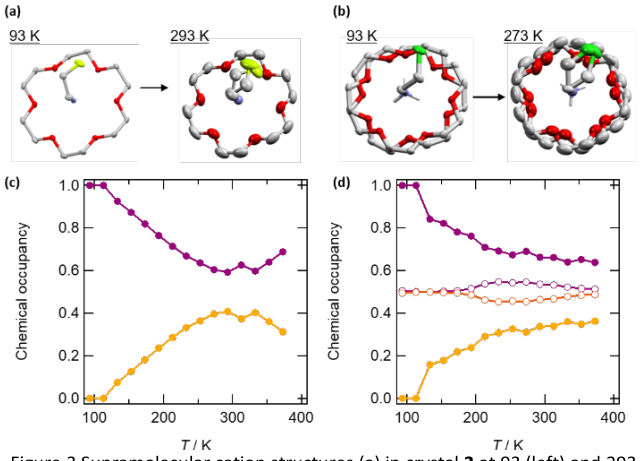

Figure 3 Supramolecular cation structures (a) in crystal **2** at 93 (left) and 293 K (right) and (b) in crystal **3** at 93 (left) and 273 K (right). Temperature dependence of occupancy of halogen atoms of X-CH_2CH_2-NH_3^+ and [18]crown-6 for (c) **2** and (d) **3**. The occupancies of halogen atoms and [18]crown-6 are shown by closed and opened circles, respectively.

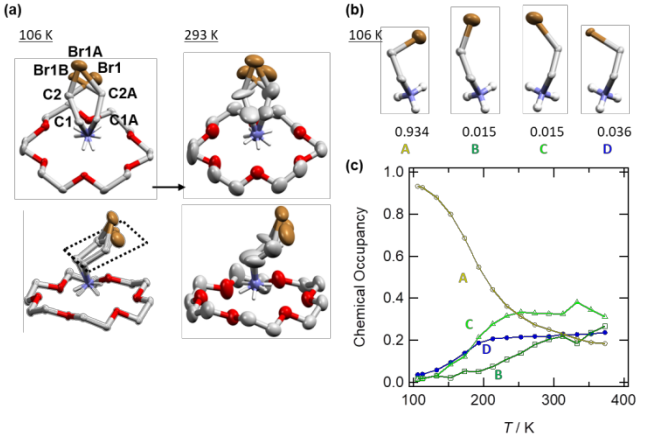

Figure 4 (a) Supramolecular cation structures in crystal **4** at 106 (left) and 293 K (right). (b) Four kinds of Br-CH_2CH_2-NH_3^+ orientations **A**-**D**. The occupancies at 106 K are indicated at the bottom. (c) Temperature dependence of the occupancies of orientations **A**-**D**.

above 200 K (Figure 3 (d)), strongly suggesting that molecular rotation of [18]crown-6 occurs at the higher temperatures like it does in the cases of $(Cs^+)_2([18]crown\text{-}6)_3[Ni(dmit)_2]^-_2$, (*p*-ammonium benzene formamide)$_2$(18-crown-6)$_3[PF_6]^-_2$ and other systems.[20,41,48] Owing to the freedom of motion of the [18]crown-6 moieties, the distance (3.782 Å) between averaged planes of adjacent [18]crown-6 is longer in crystal **3** than it is in crystals **1** (3.726 Å), **2** (3.745 Å) and **4** (3.635 Å). Moreover, the halogen containing alkyl chains in crystals **2-4** display large degrees of disorder.

Although crystal **1** does not display any significant changes with increasing temperature, other than an increase in anisotropic temperature factor, disorder between two sites exists in crystals **2** and **3**. In Figure 3 are summarized the structural changes taking place in crystals **2** and **3**, in which X-CH_2 group in X-CH_2CH_2-NH_3^+ are ordered below 93 K. In crystal **2** at 133 K, the F-CH_2 group is disordered between two sites with an occupancy ratio of 0.925(6): 0.075(6). The occupancy level at the latter site increases with increasing temperature, approaching 0.4 at 293 K (Figure 3c) and then decreasing to 0.3 at 373 K. In crystal **3**, the Cl-CH_2 groups are disordered between two sites at 133 K with an occupancy ratio of 0.842(6): 0.158(6), which gradually approaches ca. 0.6:0.4 at higher temperatures. On the other hand, the occupancy ratio of 0.5:0.5 for two [18]crown-6 sites in the crystal **3** changes only slightly from 0.55 to 0.45 above 200 K. No relationship was observed between the temperature-dependent occupancy change of the Cl-CH_2 group and [18]crown-6, suggesting that molecular motions in the supermolecule are independent. Because of the large motional freedom of both the [18]crown-6 and Cl-CH_2CH_2-NH_3^+ molecules, crystal **3** has a lower density than crystal **2** despite the fact that it contains a heavy Cl compared F atom.

Disorder of the methylene group adjacent to the amine nitrogen in addition to that of the Br-CH_2 group exist in crystal **4**. The structural changes of supramolecular cations in crystal **4** is displayed in Figure 4. The ethyl carbons are disordered between two sites (C1-C2 and C1A-C2A), and Br atoms are disordered between three sites (Br1, Br1A and Br1B). The occupancies at 106 K are 0.949(5) and 0.051(5) for C1-C2 and C1A-C2A, respectively, and 0.9342(17): 0.0364(15): 0.0294(18) for Br1, Br1A, and Br1B, respectively. Based on the covalent bond distances, at 106 K the Br-CH_2-CH_2 groups are disordered between four sites, C1-C2-Br1 (**A**), C1-C2-Br1A (**B**), C1A-C2A-Br1A (**C**), and C1A-C2A-Br1B (**D**) with occupancy ratios of 0.934: 0.015: 0.015: 0.036, respectively. The position of the Br atom is the same as that in Br2 for **B** and **C**. The C1-C2, C1A-C2A, Br1 and Br1B moieties are located in nearly the same plane, while Br1A is located out of this plane and away from the NH_3^+ group. Inspection of Figure 4c, which contains a summary of the temperature dependence of the occupancies of **A**-**D**, shows that **A** is the most stable orientation at lower temperatures. In addition, the occupancy of **B-D** increases with increasing temperature and the population of each orientation becomes nearly the same above room temperature.

The rather complex disorder existing in crystal **4** is a consequence of the greater number of different arrangements of the supramolecular structure compared to those crystals **2** and **3**. In crystals **2** and **3**, the X-CH_2 groups in two supramolecular units are oriented so as to face one other. In crystal **4**, the Br-CH_2 groups do not directly interact but are located in a space consisting of four [18]crown-6 and two $[Ni(dmit)_2]$ moieties, and where Br-CH_2-CH_2 groups have motional freedom.

To evaluate the magnitudes of the spaces that are available for molecular motion of X-CH_2-CH_2 groups in the crystals, the molecular volumes of X-CH_2-CH_2 groups (V_{vdW}) were calculated using van der Waals radii and compared with the volumes occupied by X-CH_2-CH_2 groups ($V_{X\text{-}C2}$), calculated from the internal space surrounded by the Hirshfeld surface.[49–51] While, the ratios of $V_{X\text{-}C2}$ / V_{vdW} for crystals **1** and **2** are almost the same, the ratio in crystal **3** is larger than that in crystal **2**, which may be caused by molecular motion of the [18]crown-6 moiety and the Cl-CH_2 group. Crystal **4** has the largest $V_{X\text{-}C2}$ / V_{vdW} ratio among the four crystals, which is in good agreement

with the large disorder of Br-CH_2-CH_2 groups between four sites.

Table 1. The volume occupied by the X-CH_2-CH_2 group in the crystals.

Crystal	V_{vdW} / Å^3 [a]	$V_{X\text{-}C2}$ / Å^3 [b]	$V_{X\text{-}C2}$ / V_{vdW}
1	18.83	53.94	2.86
2	20.77	54.53	2.63
3	23.68	71.53	3.02
4	24.98	80.53	3.22

a Calculated volume for one X-CH_2-CH_2 group based of van der Waals radii. *b* Internal space of Hirshfeld surface for X-CH_2-CH_2 groups.

Temperature- and Frequency-Dependent Dielectric constant

To evaluate molecular motion occurring within crystals **1**-**4**, the temperature and frequency dependencies of the dielectric constants were determined. The temperature profiles of the real part of the dielectric constants (ε_1) and the dielectric loss tangents (tan δ) of crystal **4** are given in Figure 5 (see Figure S6, S7, and S8 for dielectric properties of crystals **1**, **2**, and **3** in SI, respectively).

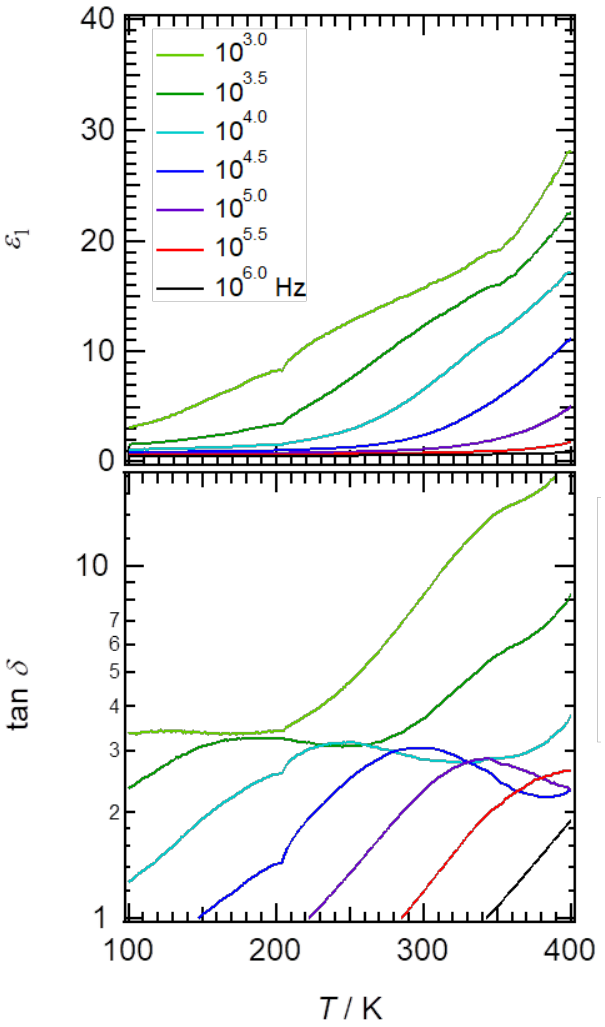

Figure 5 Temperature and frequency dependence of the real part of the dielectric constant (ε_1) and the dielectric loss tangent (tan δ) of crystal **4**.

Inspection of the plots show that the ε_1 of crystal **4** increases almost monotonically as the temperature is raised from 100 to 400 K. Corresponding changes are reflected in plots of temperature vs. tan δ, which display peaks at 189, 245, 300, 341 and 395 K for the measurement frequencies $10^{3.5}$, 10^4, $10^{4.5}$, 10^5 and $10^{5.5}$ Hz, respectively. The responses are typical of those associated with dielectric relaxation originating from molecular motion, where the temperature corresponding to a maximum value of tan δ increases with increasing frequency. The relatively slow motion of Br-CH_2-CH_2 groups associated with changing the direction of the dipole moment of crystal **4** was detected by using a low-frequency AC electric field. The occupancy rate averages as the temperature increases from 106 K. The activation energy (E_a) for dielectric relaxation is 13.1 kJ mol^{-1}, which is comparable to those for molecular motion of ethyl groups in ($CH_3CH_2NH_3^+$)[$CuCl_2$] (21.13 kJ mol^{-1}) and ($CH_3CH_2NH_3^+$)[$ZnCl_2$] (21.35 kJ mol^{-1}), estimated by utilizing relaxation times in the solid-state ^{13}C NMR.[52,53] Similar responses of tan δ to temperature arising from X-CH_2 motion occur in crystals **2** and **3**. However, because the responses in crystals **2** and **3** are one or two orders of magnitude smaller than those in crystal **4**, it was difficult to discuss relative E_a values in detail. No dielectric relaxation takes place in crystal **1**. The dielectric responses in crystals **2**-**4** are a result of changes in the direction of dipole-moments brought promoted by molecular motion. In crystal **4**, Br-CH_2-CH_2 group showed disordering, while in crystals **2** and **3**, only X-CH_2 group was disordered. Larger amplitude of molecular motion in crystal **4** should result in obvious dielectric relaxation than those in crystals **2** and **3**.

Magnetic properties

The temperature-dependencies of magnetic susceptibilities (χ_m) were measured for crystals **1**-**4**. The $\chi_m T$ versus T plots, arrived at after subtracting a contribution from a paramagnetic

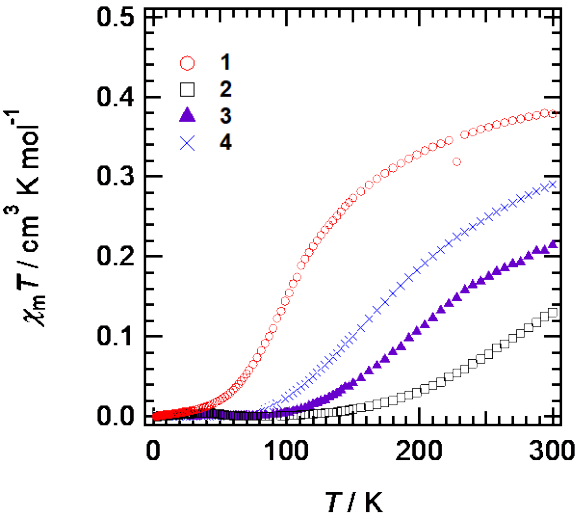

Figure 6 $\chi_m T$ *versus* T plot for crystals **1** – **4**. Red circles, black squares, purple triangles, and blue crosses correspond to the $\chi_m T$ value for crystal **1**, **2**, **3**, and **4**, respectively.

impurity, are shown in Figure 6. All crystals display relatively strong antiferromagnetic interactions. Because the magnitude of the magnetic exchange interaction ($|J|$) is proportional to the square of transfer integral (t^2),[54–56] it is useful to consider these values in gaining an understanding of the relationship between magnetic behavior and structure. The transfer integrals (t) between $[Ni(dmit)_2]^-$ are given in Fig. S9. Based on the $\chi_m T$ versus T plots, $[Ni(dmit)_2]^-$ anions in the crystals likely interact antiferromagnetically with each other. The strongest interactions take place within the $[Ni(dmit)_2]^-$ dimers with t_1 = 110, 180, 185, and 151 meV, for crystals **1**, **2**, **3** and **4**, respectively. Relatively strong interdimer interactions occur at t_3 in crystals **1** and **2**, with 15.2 and 35.8 meV respectively, which are much smaller than those in crystals **3** and **4** (4.04 and 0.09 meV, respectively). Dimer formation is the origin of the strong antiferromagnetic interactions. The magnitudes of t values are qualitatively consistent with the degree of antiferromagnetic interactions in the crystals, where the $\chi_m T$ of crystals **1**, **2**, **3** and **4** at 300 K are 0.380, 0.130, 0.214 and 0.290 cm^3 K mol^{-1}, respectively. The temperature dependence of χ_m of crystals could not be reproduced by the singlet-triplet thermal excitation model[57] even for crystals **3** and **4** in which the interdimer interactions were relatively small compared to crystals **1** and **2**.

Conclusion

Molecular motions of halogen-substituted alkylammonium moieties in crystals of $(X\text{-}CH_2CH_2\text{-}NH_3^+)$([18]crown-6)$[Ni(dmit)_2]^-$ (X = F, Cl, and Br) were assessed in the investigation summarized above. Although the ethyl groups of unsubstituted crystal **1** (X = H) do not display large amplitude motion, the corresponding haloethyl groups in crystals of **2**, **3**, and **4** exhibit distinct molecular motions associated with disorder between sites. The $X\text{-}CH_2$ moieties in crystals **2** and **3** display dynamic disorder between two sites at high temperatures. In addition, the rotational motion of [18]crown-6 occurs in crystal **3**. In crystal **4**, the $Br\text{-}CH_2\text{-}CH_2$ group is disordered between four sites. Antiferromagnetic interactions between $[Ni(dmit)_2]^-$ were observed to be present in all crystals. No correlation was observed to exist between molecular motions and magnetism. However, the morphology and size of supramolecular cations have significant effects on the arrangement and magnetic behavior of $[Ni(dmit)_2]^-$ ions.

A change in the orientation of the dipole moment in crystals is important for attaining ferroelectric, piezoelectric and pyroelectric behaviors. Results arising in this effort demonstrate the potential utility of using a supramolecular approach with crown ethers to enable molecular motion within tightly packed crystals. For example, remarkably large dielectric relaxation occurs in crystal **4** due to a change in the direction of the dipole moment promoted by molecular motion. By optimizing the crown ether and substituted alkylammonium components of supramolecular structures, it should be possible to design crystals that display unique dielectric responses including ferroelectrics. Our continuing studies in this area are aimed at utilizing this strategy to design novel multifunctional systems that advantageously utilize the relationship that exists between molecular motion and magnetism.

Conflicts of interest

There are no conflicts to declare.

Acknowledgements

We thank Dr. Xue Chen and Dr. Huang Rui-Kang of RIES, Hokkaido University, for fruitful discussions, Ms. Ai Tokumitsu of Global Facility Center, Hokkaido University for elemental analysis, Mr. Masashi Takei and Mr. Mao Kusuzaki of RIES, Hokkaido University, for making the cold head of the cryostat, and Dr. Shuhei Fukuoka and Dr. Satoaki Matsunaga of Faculty of Science, Hokkaido University for χ_m measurements. This study was supported financially by JSPS KAKENHI (grant no. JP18H01949 and JP19K15517), JST-PRESTO (grant no. JPMJPR19L3), JSPS Joint Research Projects under the Bilateral Programs, "Dynamic Alliance for Open Innovation Bridging Human, Environment and Materials", and Research Program of "Network Joint Research Center for Materials and Devices: Dynamic Alliance for Open Innovation Bridging Human, Environment and Materials" from the Ministry of Education, Culture, Sports, Science and Technology of Japan (MEXT).

Notes and references

1 H. Oki, M. Shiga, I. Nakamura, K. Nishida, K. Ichihashi, S. Nishihara, K. Inoue, T. Akutagawa and R. Tsunashima, *Eur. J. Inorg. Chem.*, 2019, **2019**, 492–495.
2 S.-Q. Su, T. Kamachi, Z.-S. Yao, Y.-G. Huang, Y. Shiota, K. Yoshizawa, N. Azuma, Y. Miyazaki, M. Nakano, G. Maruta and others, *Nat. Commun.*, 2015, **6**, 1–7.
3 S. Han, X. Liu, Y. Liu, Z. Xu, Y. Li, M. Hong, J. Luo and Z. Sun, *J. Am. Chem. Soc.*, 2019, **141**, 12470–12474.
4 W. J. Xu, P. F. Li, Y. Y. Tang, W. X. Zhang, R. G. Xiong and X. M. Chen, *J. Am. Chem. Soc.*, 2017, **139**, 6369–6375.
5 C. Ji, S. Li, F. Deng, Z. Sun, L. Li, S. Zhao and J. Luo, *J. Phys. Chem. C*, 2016, **120**, 27571–27576.
6 T. Minami, H. Sato and S. Matsumoto, *CrystEngComm*, 2018, **20**, 2644–2647.
7 Z. H. Wei, Z. T. Jiang, X. X. Zhang, M. L. Li, Y. Y. Tang, X. G. Chen, H. Cai and R. G. Xiong, *J. Am. Chem. Soc.*, 2020, **142**, 1995–2000.
8 H. L. Cai, Y. Zhang, D. W. Fu, W. Zhang, T. Liu, H. Yoshikawa, K. Awaga and R. G. Xiong, *J. Am. Chem. Soc.*, 2012, **134**, 18487–18490.
9 D. W. Fu, W. Zhang, H. L. Cai, J. Z. Ge, Y. Zhang and R. G. Xiong, *Adv. Mater.*, 2011, **23**, 5658–5662.
10 D. W. Fu, H. L. Cai, Y. Liu, Q. Ye, W. Zhang, Y. Zhang, X. Y. Chen, G. Giovannetti, M. Capone, J. Li and R. G. Xiong, *Science (80-.).*, 2013, **339**, 425–428.
11 R. Jakubas, A. Gągor, M. J. Winiarski, M. Ptak, A. Piecha-Bisiorek and A. Ciżman, *Inorg. Chem.*, 2020, 59, 3417–3427.
12 S.-S. Wang, X.-X. Chen, B. Huang, R.-K. Huang, W.-X. Zhang and X.-M. Chen, *CCS Chem.*, 2019, **1**, 448–454.

13 A. M. Rich, S. Bhattacharyya, V. R. Aldilla, J. E. Beves, M. Bhadbhade, N. Kumar, E. T. Luis and C. E. Marjo, *J. Raman Spectrosc.*, 2019, **50**, 63–73.
14 X. N. Hua, W. Q. Liao, Y. Y. Tang, P. F. Li, P. P. Shi, D. Zhao and R. G. Xiong, *J. Am. Chem. Soc.*, 2018, **140**, 12296–12302.
15 W. Guo, X. Liu, S. Han, Y. Liu, Z. Xu, M. Hong, J. Luo and Z. Sun, *Angew. Chemie*, 2020, **132**, 13983–13988.
16 Y. Xiong, T. Sha, Q. Pan, X. Song, S. Miao, Z. Jing, Z. Feng, Y. You and R. Xiong, *Angew. Chemie Int. Ed.*, 2019, **58**, 8857–8861.
17 Y.-M. You, W.-Q. Liao, D. Zhao, H.-Y. Ye, Y. Zhang, Q. Zhou, X. Niu, J. Wang, P.-F. Li, D.-W. Fu, Z. Wang, S. Gao, K. Yang, J.-M. Liu, J. Li, Y. Yan and R.-G. Xiong, *Science (80-.).*, 2017, **357**, 306–309.
18 Y. Zhang, X. J. Song, Z. X. Zhang, D. W. Fu and R. G. Xiong, *Matter*, 2020, **2**, 697–710.
19 T. Akutagawa, K. Shitagami, M. Aonuma, S. I. Noro and T. Nakamura, *Inorg. Chem.*, 2009, **48**, 4454–4461.
20 T. Akutagawa, D. Endo, F. Kudo, S.-I. Noro, S. Takeda, L. Cronin and T. Nakamura, , DOI:10.1021/cg060951.
21 T. Akutagawa, D. Sato, H. Koshinaka, M. Aonuma, S. I. Noro, S. Takeda and T. Nakamura, *Inorg. Chem.*, 2008, **47**, 5951–5962.
22 T. Nakamura, T. Akutagawa, K. Honda, A. E. Underhill, A. T. Coomber and R. H. Friend, *Nature*, 1998, **394**, 159–162.
23 Y. Shirakawa, K. Takahashi, H. Sato, N. Hoshino, H. Anetai, S. Noro, T. Akutagawa and T. Nakamura, *Chem. – A Eur. J.*, 2019, **25**, 6920–6927.
24 C. S. Vogelsberg and M. A. Garcia-Garibay, *Chem. Soc. Rev.*, 2012, **41**, 1892–1910.
25 S. Pérez-Estrada, B. Rodríguez-Molina, E. F. Maverick, S. I. Khan and M. A. Garcia-Garibay, *J. Am. Chem. Soc.*, 2019, **141**, 2413–2420.
26 I. Liepuoniute, C. M. Huynh, S. Perez-Estrada, Y. Wang, S. Khan, K. N. Houk and M. A. Garcia-Garibay, *J. Phys. Chem. C*, 2020, **124**, 15391–15398.
27 T. Masuda, J. Arase, Y. Inagaki, M. Kawahata, K. Yamaguchi, T. Ohhara, A. Nakao, H. Momma, E. Kwon and W. Setaka, *Cryst. Growth Des.*, 2016, **16**, 4392–4401.
28 J. E. Nuñez, A. Natarajan, S. I. Khan and M. A. Garcia-Garibay, *Org. Lett.*, 2007, **9**, 3559–3561.
29 W. Setaka, K. Inoue, S. Higa, S. Yoshigai, H. Kono and K. Yamaguchi, *J. Org. Chem.*, 2014, **79**, 8288–8295.
30 W. Setaka and K. Yamaguchi, *J. Am. Chem. Soc.*, 2013, **135**, 14560–14563.
31 I. Liepuoniute, M. J. Jellen and M. A. Garcia-Garibay, *Chem. Sci.*, , DOI:10.1039/d0sc04495d.
32 J. Perego, S. Bracco, M. Negroni, C. X. Bezuidenhout, G. Prando, P. Carretta, A. Comotti and P. Sozzani, *Nat. Chem.*, 2020, **12**, 845–851.
33 M. D. E. Forbes, M. A. Garcia-Garibay, M. J. Jellen, M. J. Ayodele and A. Cantu, *J. Am. Chem. Soc.*, 2020, **142**, 18513–18521.
34 D.-W. W. Fu, H.-L. L. Cai, S.-H. H. Li, Q. Ye, L. Zhou, W. Zhang, Y. Zhang, F. Deng and R.-G. G. Xiong, *Phys. Rev. Lett.*, 2013, **110**, 257601.
35 Y. Chen, Y. Liu, B. Gao, C. Zhu and Z. Liu, *Crystals*, , DOI:10.3390/cryst7070224.
36 H. Y. Zhang, S. Q. Lu, X. Chen, R. G. Xiong and Y. Y. Tang, *Chem. Commun.*, 2019, **55**, 11571–11574.
37 W. Q. Liao, Q. Q. Zhou, P. F. Li and Y. Zhang, *Chinese Chem. Lett.*, 2014, **25**, 723–726.
38 T. Akutagawa, D. Sato, Q. Ye, T. Endo, S. Noro, S. Takeda and T. Nakamura, *Dalt. Trans.*, 2010, **39**, 8219–8227.
39 F. F. Wang, C. Chen, Y. Zhang and D. W. Fu, *Chinese Chem. Lett.*, 2015, **26**, 31–35.
40 H. Y. Liu, H. Y. Zhang, X. G. Chen and R. G. Xiong, *J. Am. Chem. Soc.*, 2020, 142, 15205–15218.
41 Y. Liu, H. T. Zhou, S. P. Chen, Y. H. Tan, C. F. Wang, C. S. Yang, H. R. Wen and Y. Z. Tang, *Dalt. Trans.*, 2018, **47**, 3851–3856.
42 T. Akutagawa, H. Koshinaka, D. Sato, S. Takeda, S.-I. Noro, H. Takahashi, R. Kumai, Y. Tokura and T. Nakamura, *Nat. Mater.*, 2009, **8**, 342–347.
43 T. Akutagawa and T. Nakamura, *Dalt. Trans.*, 2008, **45**, 6335–6345.
44 G. Steimecke, H.-J. Sieler, R. Kirmse and E. Hoyer, *Phosphorous Sulfur Relat. Elem.*, 1979, **7**, 49–55.
45 G. M. Sheldrick, *Acta Crystallogr. Sect. A Found. Adv.*, 2015, **71**, 3–8.
46 O. V Dolomanov, L. J. Bourhis, R. J. Gildea, J. A. K. Howard and H. Puschmann, *J. Appl. Crystallogr.*, 2009, **42**, 339–341.
47 T. Mori, A. Kobayashi, Y. Sasaki, H. Kobayashi, G. Saito and H. Inokuchi, *Bull. Chem. Soc. Jpn.*, 1984, **57**, 627–633.
48 T. Akutagawa, K. Shitagami, S. Nishihara, S. Takeda, T. Hasegawa, T. Nakamura, Y. Hosokoshi, K. Inoue, S. Ikeuchi, Y. Miyazaki and K. Saito, *J. Am. Chem. Soc.*, 2005, **127**, 4397–4402.
49 P. A. Wood, J. J. McKinnon, S. Parsons, E. Pidcock and M. A. Spackman, *CrystEngComm*, 2008, **10**, 368–376.
50 M. A. Spackman and D. Jayatilaka, *CrystEngComm*, 2009, **11**, 19–32.
51 S. L. Tan, M. M. Jotani and E. R. T. Tiekink, *Acta Crystallogr. Sect. E Crystallogr. Commun.*, 2019, **75**, 308–318.
52 A. R. Lim, *RSC Adv.*, 2019, **9**, 38032–38037.
53 A. R. Lim and Y. L. Joo, *RSC Adv.*, 2018, **8**, 34110–34115.
54 J. C. Scott, *Semiconductors and Semimetals: Highly Conducting Quasi One-dimensional Organic Crystals*, Academic Press, San Diego, 1988.
55 T. Akutagawa, T. Nakamura, T. Inabe and A. E. Underhill, *Thin Solid Films*, 1998, **331**, 264–271.
56 T. Akutagawa and T. Nakamura, *Coord. Chem. Rev.*, 2002, **226**, 3–9.
57 C. P. Landee and M. M. Turnbull, *J. Coord. Chem.*, 2014, **67**, 375–439.